N-substituted carbamates syntheses with alkyl carbamates as carbonyl source over Ni-promoted Fe₃O₄ catalyst

Jianpeng Shang [a,b], Xiaoguang Guo [a], Feng Shi [a,*], Yubo Ma [a,b], Feng Zhou [a,b], Youquan Deng [a,*]

[a] *Centre for Green Chemistry and Catalysis, Lanzhou Institute of Chemical Physics, Chinese Academy of Sciences, Lanzhou 730000, China*
[b] *Graduate School of the Chinese Academy of Sciences, Beijing 100039, China*

ARTICLE INFO

ABSTRACT

A series of catalysts of magnetic iron oxide containing Ni with different nickel content were prepared with co-precipitation method and tested in the syntheses of N-substituted carbamates from various amines and alkyl carbamates. Under the optimized reaction conditions, various N-substituted carbamates were successfully synthesized with 90–98% isolated yield. The catalyst could be recovered based on the magnetic property of the catalyst and reused for five runs without deactivation. The catalysts were characterized with X-ray photoelectron spectroscopy, X-ray diffraction, temperature-programmed reduction, temperature-programmed desorption, and Mössbauer spectroscopy analyses. The results showed that the catalytic activity may be derived from the delicate synergy between Ni and Fe species resulted in specific basic sites. Quasi in situ FT-IR and isotopic tracer revealed that the formation of substituted urea was the key step and the N-substituted carbamate was formed via further alcoholysis of the substituted urea.

1. Introduction

Isocyanates are major raw materials for the manufacture of polyurethane, which have widely been used in producing elastomer, elastic fiber, coatings, and so on [1–3]. Now, isocyanates are produced on a commercial scale using extremely toxic phosgene as the carbonyl source [4,5]. Thus, there have been increasing interests in developing green alternative methods for isocyanate production. One of the most attractive non-phosgene processes is the thermal cleavage of N-substituted carbamates to obtain corresponding isocyanates [6–8]. However, the most N-substituted carbamates have been synthesized using isocyanates as starting material [9–11]. Thus, developing environmentally friendly and economically favorable methods for the syntheses of N-substituted carbamates is the vital step to realize the non-phosgene manufacturing of isocyanates. Meanwhile, N-substituted carbamates also represent an important class of compounds showing various interesting properties. They have wide utility in various areas including pharmaceuticals, agrochemicals, protection of amino group in peptide chemistry, and as linkers in combinatorial chemistry [12–14].
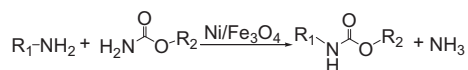
Up to now, great efforts have been made to explore environmentally benign methods for N-substituted carbamates syntheses. There are several alternative non-phosgene routes for N-substituted carbamates syntheses with different carbonyl sources. Transitional metal complexes–catalyzed carbonylation of nitroaromatics or amines with carbon monoxide have been extensively studied [15–17]. Also, dimethyl carbonate (DMC) as an attractive eco-friendly alternative to phosgene has attracted extensive attentions and good results were reported [18–20]. However, the intrinsic problems such as poisonous carbon monoxide, higher cost of transitional metal complexes, and higher price of DMC limit their practical applications. Apart from carbon monoxide and DMC, CO₂ is also a potential phosgene substitute, which has the advantages of being non-toxic, abundant, and economical. Theoretically, CO₂ should be the ideal carbonyl source in carbonylation reactions [21,22]. Unfortunately, the high chemical inertness of CO₂ limits its practical use in carbonylation processes. Normally, the activation of CO₂ needs unsaturated compounds, small-membered ring compounds, and organometallics or needs to shift the equilibrium to the product side via removing a co-produced product [23–25]. Until now, urea manufacturing is the only way for the large-scale chemical fixation of CO₂ [26,27].

Alkyl carbamates, e.g., methyl carbamate (MC), ethyl carbamate (EC), and butyl carbamate (BC), which can be produced with urea alcoholysis, are promising green carbonyl source with lower cost [28,29]. Also, the co-produced NH₃ could be recycled for urea production. Therefore, the use of CO₂ as carbonyl source could be realized. In this way, alkyl carbamates could be developed into a green and economical carbonyl source besides phosgene, carbon monoxide, and DMC. Possibly, it might be a new carbonyl source for future. Till now, various metal salts, such as ZnCl₂, FeCl₃, Y(NO₃)₃, have been reported as catalysts for the catalytic syntheses of

R₁–NH₂ + H₂N–C(=O)–O–R₂ →(Ni/Fe₃O₄) R₁–NH–C(=O)–O–R₂ + NH₃

$$R_1\text{-}NH_2 + H_2N\overset{O}{\underset{}{\|}}C\text{-}O\text{-}R_2 \xrightarrow{Ni/Fe_3O_4} R_1\underset{H}{N}\overset{O}{\underset{}{\|}}C\text{-}O\text{-}R_2 + NH_3$$

Scheme 1. N-substituted carbamate synthesis from alkyl carbamate and amine.

N-substituted carbamates from amines and alkyl carbamates [30–33]. However, the lower efficiency, separation, and recovery problems of the catalysts are still maintained as the major problems.

Since magnetic particles have emerged as a useful group for heterogeneous catalysts because of their good stability and easy separability with external magnetic field [34,35], herein, we report the preparation of magnetic iron oxide containing Ni as highly effective and recoverable catalyst for N-substituted carbamates syntheses with amines and alkyl carbamates, Scheme 1.

2. Experimental

All chemicals used in the experiments were of analytical grade and were used without further purification otherwise specified. The methanol, ethanol, and butanol used as solvents were dehydrated by 4A molecular sieves and purified with distillation before use.

2.1. Catalysts preparation

A series of catalysts of iron oxide containing Ni were prepared by co-precipitation method using $Ni(NO_3)_2 \cdot 6H_2O$ and $Fe(NO_3)_3 \cdot 9H_2O$ as starting materials and Na_2CO_3 as precipitant. At room temperature, an aqueous solution containing 20.2 g (50 mmol) $Fe(NO_3)_3 \cdot 9H_2O$, and 0–2.09 g (0–7.2 mmol) $Ni(NO_3)_2 \cdot 6H_2O$ was added dropwise into 300 mL of Na_2CO_3 solution (0.47 mol/L) with vigorous stirring. After filtration and washing with 80–100 mL of distilled water, the resulted precipitates were dried at 120 °C for 16 h. Then, precursors were calcined at 400 °C for 5 h and finally reduced under H_2 flow at 400 °C for 2 h. In the end, ~4.0 g Ni/Fe_3O_4 catalysts with 0–5.1 wt.% nickel content were obtained. The calcined, reduced, and used five times catalysts were denoted as Ni/Fe_2O_3, Ni/Fe_3O_4, and used Ni/Fe_3O_4, respectively. Pure Fe_2O_3 and NiO were prepared in the similar manner to Ni/Fe_2O_3, and Fe_3O_4 and NiO_x were prepared via further reduction of Fe_2O_3 and NiO with H_2 at 400 °C for 2 h.

2.2. Catalysts characterization

The nickel content in catalysts was determined with ICP-AES (IRIS Advantage ER/S). The BET surface areas, pore volumes, and average pore diameters of catalysts were obtained with physisorption of N_2 using a Micromeritics ASAP 2010. X-ray photoelectron spectroscopy (XPS) analysis was carried out using a VG ESCALAB 210 instrument with Mg Kα radiation (1253.6 eV), and all the binding energies were referenced to the adventitious C 1s at 285 eV. X-ray diffraction (XRD) measurements were carried out on a Siemens D/max-RB powder X-ray diffractometer. Diffraction patterns were recorded with Cu Kα radiation (40 mA, 40 kV) over a 2θ range of 15–80°.

Temperature-programmed reduction (TPR) of H_2 was carried out on TPR/TPD flow system equipped with an MS detector (DM300, AMETEK, USA). TPR analysis was conducted with 10% H_2/Ar (50 mL min^{-1}). In a typical experiment, the solid sample (150 mg with particle size 160–200 μm) was pretreated at 400 °C for 1 h under air flow (50 mL min^{-1}) and then cooled to room temperature under argon gas flow (50 mL min^{-1}). The profile was recorded at a heating rate of 10 °C min^{-1} from room temperature to 700 °C and maintained at this temperature until the MS signal of H_2 returned to the baseline.

The Mössbauer spectra were obtained at room temperature with a Wissel (Wissenschaftliche Elektronik GmbH, Germany) electromechanical spectrometer working in a constant acceleration mode. A ^{57}Co/Pd (activity ≅ 25 m Ci) source and α-Fe standard were used. The experimentally obtained spectra were fitted to mathematical processing according to the least squares method. The parameters of hyperfine interaction such as isomer shift (IS), quadrupole splitting (QS), hyperfine magnetic field (H_{hf}), and the relative area of the partial components in the spectra were determined.

Temperature-programmed desorption (TPD) of CO_2 and NH_3 was conducted to study the acid–base properties of the catalyst. In a typical experiment, the solid sample (100 mg with particle size 160–200 μm) was pretreated at 400 °C for 1 h under nitrogen flow (50 mL min^{-1}) and then cooled to room temperature. The sample was subsequently exposed to CO_2 (NH_3) stream (50 mL min^{-1}) at room temperature for 1 h and flushed again with nitrogen for 1 h to remove any physico-adsorbed CO_2 (NH_3). The desorption profile was recorded at a heating rate of 10 °C min^{-1} from room temperature to 400 °C and maintained at this temperature until the MS signal of CO_2 (NH_3) returned to the baseline.

The quasi in situ FT-IR spectroscopic study was performed in a closed stainless steel cell equipped with KBr windows for reacting and scanning at proper temperatures, and the spectra were recorded on a Nicolet 5700 Fourier transform infrared spectrometer in the region of 4000–400 cm^{-1} with a resolution of 4 cm^{-1}. In a typical experiment, the sample was prepared by mixing catalyst (10 mg 5.1 wt.% Ni/Fe_3O_4), 4,4′-methylenedianiline (MDA) (1 mmol), and EC (7 mmol), and then 1 mg samples and 200 mg KBr were ground finely and pressed into a thin disk and the disk was put into the closed cell. Two types of experiments were carried out: (a) without addition of alcohol into the cell and (b) with the addition of alcohol into the cell, which was injected at 110 °C with 20 μL. Moreover, butanol (due to higher b.p. of butanol which would be favorable for experimental operation but not affect reaction mechanism) instead of ethanol was used and injected into the cell during reaction and was not pressed into the KBr disk.

The isotopic labeling studies were performed with d_4-labeled methanol. 0.5 mmol aniline, 0.5 mmol MC, 5 mmol d_4-methanol, and 5 mg 5.1 wt.% Ni/Fe_3O_4 were added into a 20 mL pressure tube (Aldrich–Sigma). Then, it was sealed and reacted at 190 °C for 1 h. Also, reaction with equal amount of d_4-methanol (10 mmol) and methanol (10 mmol), 0.5 mmol aniline, 0.5 mmol MC, and 5 mg 5.1 wt.% Ni/Fe_3O_4 were tested to investigate the isotope effect.

2.3. Catalytic activity measurement

All reactions were carried out in a 90 mL stainless steel autoclave with a glass tube inside and with magnetic stirring. Amines such as 1,6-hexamethylenediamine (HDA), isophorondiamine, 4,4′-methylenedicyclohexanamine, dodecylamine, allylamine, MDA, 2,4-diaminotoluene and benzylamine, and alkyl carbamates such as MC, EC, and BC were used as substrates. Typically, 10 mmol amine, 70 mmol alkyl carbamate, 170 mmol alcohol, and 100 mg catalyst were added. Under nitrogen atmosphere, the reaction proceeded at 190 °C and 1.5–2.2 MPa pressures for 5–12 h. After reaction, the autoclave was cooled down to room temperature. The catalyst was separated and recovered using an external magnetic field. Pure compounds and corresponding isolated yields were obtained with different procedures. (I) diamines as substrates: ~25 mL alcohol (methanol, ethanol, or butanol was used for reactions using MC, EC, or BC as carbonyl source, respectively) was added into the reacted mixture to dissolve the product and unreacted alkyl carbamate, and the unsolvable by-products were removed by filtration. Then, the alcohol and alkyl carbamate were removed with a rotary evaporator under vacuum and raw solid

product was obtained. It was further washed with diethyl ether/hexane to remove alcohol residue and soluble impurities, and desired pure product was obtained and weighted; (II) monoamines as substrates: ~25 mL ethanol was added into the reacted mixture to dissolve the products and unreacted EC, and the unsolvable by-product was removed by filtration. Then, ethanol was removed under vacuum and ~100 mL of distilled water was added into the mixture of EC and product to dissolve the unreacted EC. After filtration, the raw solid product was further washed with diethyl ether/hexane to remove ethanol residue and soluble impurities and desired product was obtained and weighted.

2.4. Qualitative and quantitative analyses and identification

The qualitative and quantitative analyses of the resulted liquid mixtures were conducted with GC–MS (Agilent 6890/5973) and GC (Agilent 6820) equipped with a FID detector using biphenyl as an internal standard. All the products were also identified with ^{1}H NMR (Bruker AMX FT 400-MHz) and ^{13}C NMR (Bruker AMX FT 100-MHz).

3. Results and discussion

3.1. Characterization of catalysts

The physical properties of the catalysts are summarized in Table 1. The BET surface area of pure NiO_x is 1.8 m²/g, which is much smaller than that of the iron oxide, entries 1 and 2. Clearly, the BET surface area changed greatly after 5.0 wt.% Ni/Fe₂O₃ catalyst was reduced with H_2 at 400 °C, which decreased from 47.6 to 9.6 m²/g, entries 4 and 5. In comparison with the surface area of fresh 5.1 wt.% Ni/Fe₃O₄, the BET surface area of the used 5.1 wt.% Ni/Fe₃O₄ increased to 15.2 m²/g, entry 6. This might be due to the partial re-oxidation of the catalyst during the reaction, which will be further discussed in the following paragraphs. Moreover, the BET surface area of the samples with different nickel content showed that the nickel content has no effect on the BET surface area.

The XPS spectra (Fig. 1a and b) of the fresh and used 5.1 wt.% Ni/Fe₃O₄ showed that the binding energies of Fe 2p$_{3/2}$ and Ni 2p$_{3/2}$ were 710.7, 711.4, 855.3, and 856.7 eV, respectively, suggesting that the chemical states of Fe and Ni species on the catalyst surface were mainly Fe^{3+} and Ni^{2+} although the catalyst was reduced with H_2 at elevated temperatures [36,37], and Ni species may be highly dispersed on the iron oxide since the binding energies of Ni 2p$_{3/2}$ (855.3 and 856.7 eV) were remarkably higher than that of standard NiO (B.E. of Ni 2p$_{3/2}$ = 853.8 eV). After the 5.1 wt.% Ni/Fe₃O₄ was used for five times, the binding energies of Fe 2p$_{3/2}$ and Ni 2p$_{3/2}$ were slightly higher that of the fresh 5.1 wt.% Ni/Fe₃O₄, suggesting some extent of oxidation of the catalyst surface. Two O 1s peaks at 530.4 and 531.4 eV were found over the fresh 5.1 wt.% Ni/Fe₃O₄ (Fig. 1c), and three O 1s peaks at 530.4, 531.8, and 533.3 eV were observed over the used 5.1 wt.% Ni/Fe₃O₄, i.e., a new kind of O

Table 1
Physicochemical properties of the iron oxide containing Ni catalysts.

Entry	Catalysts	S_{BET} (m²/g)	d_p^a (nm)	v_p^b (cm³/g)	Total basic sites (μmol/g)
1	NiO_x	1.8	31.9	0.01	5
2	Fe₃O₄	9.5	25.6	0.05	32
3	3.2 wt.% Ni/Fe₃O₄	9.5	24.8	0.05	43
4	5.1 wt.% Ni/Fe₃O₄	9.6	23.6	0.05	52
5	5.0 wt.% Ni/Fe₂O₃	47.6	19.4	0.25	102
6	Used 5.1 wt.% Ni/Fe₃O₄	15.2	18.3	0.09	58

^{a} Average pore size.
^{b} Average pore volume.

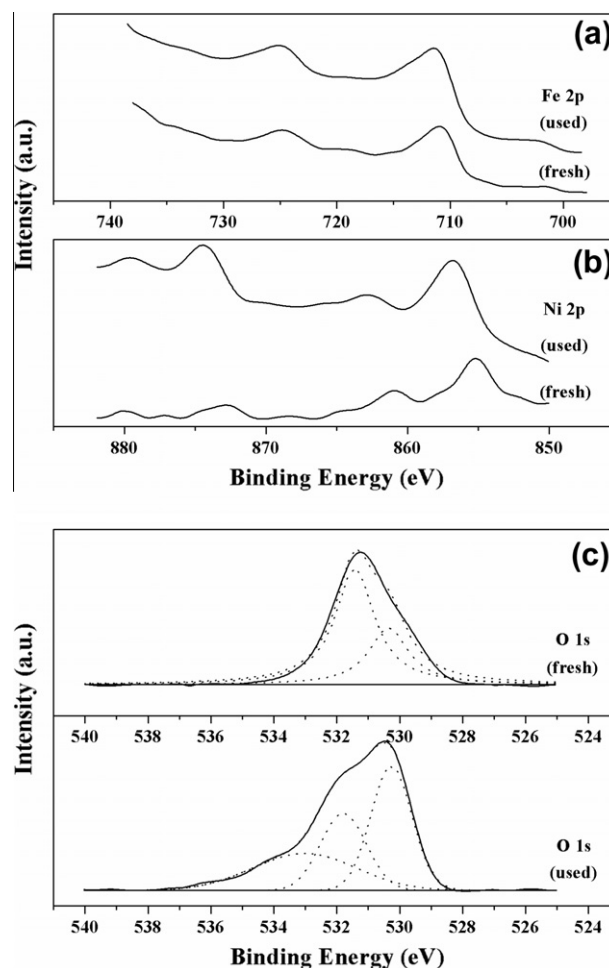**Fig. 1.** XPS spectra of: (a) Fe 2p spectra of fresh and used 5.1 wt.% Ni/Fe₃O₄, (b) Ni 2p spectra of fresh and used 5.1 wt.% Ni/Fe₃O₄ and (c) O 1s spectra of fresh and used 5.1 wt.% Ni/Fe₃O₄.

species (B.E. = 533.3 eV) was formed, which may be derived from OH species or chemisorbed water formed during the reactions [38,39]. Furthermore, the surface atom ratio of Ni/Fe over the fresh 5.1 wt.% Ni/Fe₃O₄ was 0.03, which was lower than that of the corresponding bulk composition (0.07). For the used 5.1 wt.% Ni/Fe₃O₄, however, the surface atom ration of Ni/Fe was 0.05, which was slightly higher than that of the fresh one. These results showed that the Ni species might be encapsulated with Fe₃O₄ in the fresh catalyst and the Ni species were slightly enriched on the surface of the used catalyst.

XRD patterns of pure Fe₃O₄, 3.2 wt.% Ni/Fe₃O₄, fresh and used 5.1 wt.% Ni/Fe₃O₄ are shown in Fig. 2. The results showed that the characteristic diffraction peaks of Fe₃O₄ were observed for all samples and confirmed the Fe₃O₄ formation. For 3.2 wt.% and fresh 5.1 wt.% Ni/Fe₃O₄ (Fig. 2b and c), the XRD results indicated that the Ni species were highly dispersed on the iron oxide as the characteristic diffraction peaks of NiO (2θ = 43.3°, 37.3°, and 62.9°) and Ni (2θ = 44.5°, 51.8°, and 76.4°) cannot be discerned. In addition to Fe₃O₄ phase, a peak at 44.7° (d = 2.028 Å) also exists, which may be ascribed to the Fe^0 phase or bcc Fe–Ni alloy, and the intensity of such diffraction peak was enhanced and increased with the increasing nickel content. This is different from the observation with XPS. Possibly, the Fe^0 or bcc Fe–Ni alloy on the surface of the catalyst was oxidized into iron oxide again in air. This result suggested that the presence of Ni would promote the formation of crystal Fe^0 or bcc Fe–Ni alloy. For used 5.1 wt.% Ni/Fe₃O₄

Fig. 2. XRD patterns of: (a) Fe_3O_4, (b) 3.2 wt.% Ni/Fe_3O_4, (c) 5.1 wt.% Ni/Fe_3O_4 and (d) used 5.1 wt.% Ni/Fe_3O_4.

Fig. 3. TPR-H_2 profiles of: (a) Ni oxide, (b) Fe_2O_3 and (c) 5.0 wt.% Ni/Fe_2O_3.

Fig. 4. Mössbauer spectra of: (a) Fe_3O_4 and (b) 5.1 wt.% Ni/Fe_3O_4, recorded at room temperature.

Table 2
Mössbauer parameters of Fe_3O_4 and 5.1 wt.% Ni/Fe_3O_4 at room temperature.

Sample	Component	IS (mm/s)	QS (mm/s)	H_{hf} (T)	Area (%)
Fe_3O_4	Fe_3O_4 (A)	0.24	−0.09	49.70	50.7
	Fe_3O_4 (B)	0.73	0.09	47.38	45.4
	Fe^{2+}	0.59	2.37		3.9
5.1 wt.% Ni/Fe_3O_4	Fe_3O_4 (A)	0.29	0	49.85	21.6
	Fe_3O_4 (B)	0.64	0.02	46.65	25.4
	Fe^{3+}	0.4	0.75		8.9
	Fe	−0.01	0	33.94	44.2

The Mössbauer spectra at room temperature for the Fe_3O_4 and 5.1 wt.% Ni/Fe_3O_4 are shown in Fig. 4, and the Mössbauer parameters are listed in Table 2. The raw spectra of Fe_3O_4 can be fitted to two sextets and one paramagnetic doublet, Fig. 4a. The outer sextet with IS = 0.24 mm/s was assigned to high spin Fe^{3+} on the tetrahedral sites, denoted as Fe_3O_4 (A) in Table 2. The inner sextet with IS = 0.73 mm/s was associated with a mixture of Fe^{2+} and Fe^{3+} on the octahedral sites, brought about by rapid electron exchange between both kinds of cations at room temperature, denoted as Fe_3O_4 (B) in Table 2 [42]. The doublet peak with IS = 0.59 mm/s and QS = 2.37 mm/s can be ascribed to high spin Fe^{2+}, which may be formed during the hydrogen reduction process [43]. For 5.1 wt.% Ni/Fe_3O_4, the raw spectra can be fitted to three sextets and one paramagnetic doublet. Among the three sextets, two sextets with IS = 0.29 mm/s and IS = 0.64 mm/s were attributed to the Fe_3O_4 (A) and Fe_3O_4 (B), respectively. Beside those two sextets, another sextet with IS = −0.01 mm/s was the characteristic sextet of metallic Fe. However, the value of H_{hf} (H_{hf} = 33.94 T) was higher than that of the pure metallic Fe (H_{hf} = 33 T), which indicated that the coordination environment of the Fe atom was changed and may be due to the formation of Fe–Ni alloy. According to the date from reference [44] for bcc Fe–Ni alloys, it was assumed that one Ni atom increases the H_{hf} by 0.94 T when it substitutes Fe atom in the first coordination sphere. Thus, it can be conjectured that there is one Ni atom as the nearest neighbor of the Fe atom. Those results showed that the bcc Fe–Ni alloy was formed after the nickel species were introduced into the iron oxide and the diffraction peak at 44.7° in the XRD could be assigned to Fe–Ni alloy phase. The doublet peak with IS = 0.40 mm/s and QS = 0.75 mm/s was related to the high spin Fe^{3+} [43]. Moreover, the presence of Fe–Ni alloy after the nickel species was introduced, suggesting that addition of nickel component favored the reduction of the iron oxide, which is consistent with the results of TPR. Based on the results of

(Fig. 2d), the intensity of the Fe^0 or bcc Fe–Ni alloy characteristic diffraction peak slightly decreased probably due to the re-oxidation of the reduced Fe species during the reaction.

TPR results of Ni oxide, Fe_2O_3, and 5.0 wt.% Ni/Fe_2O_3 are shown in Fig. 3. For Ni oxide, two reduction peaks at 265 and 351–370 °C were observed, which could be attributed to the surface and bulk reduction of Ni oxide, respectively [40]. For Fe_2O_3, a sharp peak centered at 468 °C and a broad peak at 622 °C along with a shoulder at 700 °C were observed. The peak at 468 °C is assigned to the reduction of Fe_2O_3 to Fe_3O_4 [41]. The peak at 622 °C can be ascribed to a subsequent reduction of Fe_3O_4 and ultimately involving the formation of metallic iron [41]. Three reduction peaks at 362, 441, and 616 °C were found over 5.1 wt.% Ni/Fe_2O_3. In comparison with TPR profiles of pure NiO (351 °C) and Fe_2O_3 (468 °C), the peak at 362 °C should be attributed to the reduction of nickel oxide species in the catalyst. The shift in the reduction temperature from 351 to 362 °C suggested that there may be a strong interaction between nickel species and iron oxide support. Furthermore, the shift in the reduction temperature from 468 to 441 °C also indicated that some sort of interaction occurred between nickel species and iron oxide and addition of nickel component favored the reduction of the iron oxide.
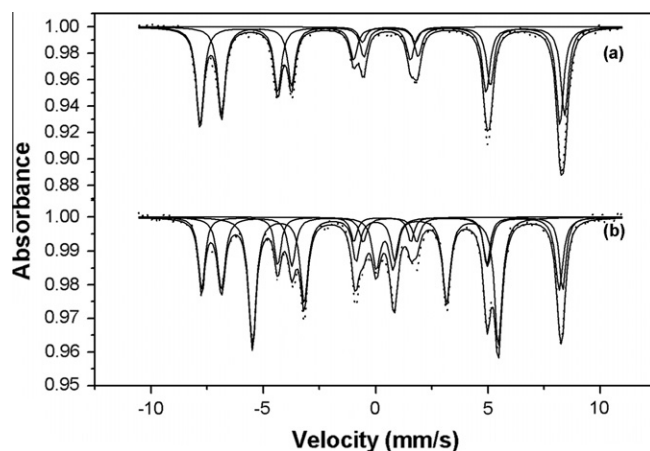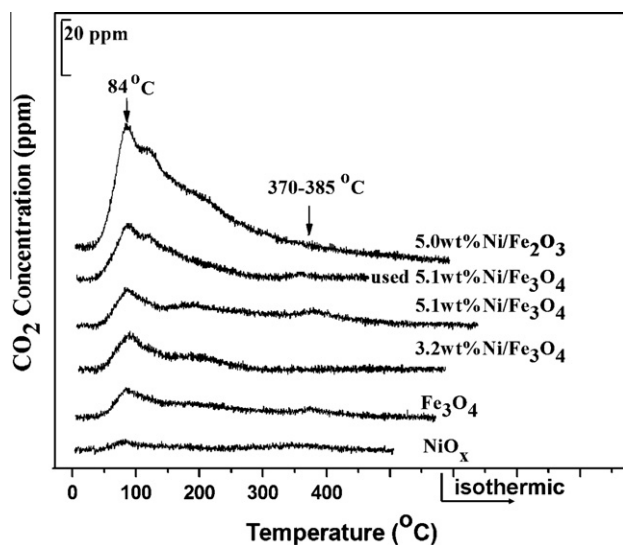
Fig. 5. TPD-CO_2 profiles of: (a) NiO_x, (b) Fe_3O_4, (c) 3.2 wt.% Ni/Fe_3O_4, (d) 5.1 wt.% Ni/Fe_3O_4, (e) used 5.1 wt.% Ni/Fe_3O_4 and (f) 5.0 wt.% Ni/Fe_2O_3.

characterizations, the catalyst system is in fact Ni (partially or fully reduced to metallic Ni) dispersed on magnetic iron oxide.

The TPD-CO_2 results of NiO_x, Fe_3O_4, 3.2 wt.% Ni/Fe_3O_4, fresh and used 5.1 wt.% Ni/Fe_3O_4, and 5.0 wt.% Ni/Fe_2O_3 are shown in Fig. 5. Generally, two peaks of CO_2 desorption were observed over the tested samples. The first peak appeared at about 84 °C, which was derived from the weak strength basic sites. The second broad peak was observed about 370–385 °C, which was attributed to medium strength basic sites. In comparison with the fresh 5.1 wt.% Ni/Fe_3O_4, TPD-CO_2 profile of the used catalyst has almost no difference. From the quantitative results of TPD-CO_2 (Table 1), it can be seen that the total basic sites increased from 32 to 52 µmol/g for pure Fe_3O_4 and 5.1 wt.% Ni/Fe_3O_4, respectively, when nickel component was added and nickel content was increased. Meanwhile, the amounts of medium strength basic sites were much lower than that of weak strength basic sites and the nickel species have little effect on the amount of the medium strength basic sites, which suggested that the peak of CO_2 desorption at high temperature should not be related to the catalytic activity, but to the formation of the strongly bound carbonates during the absorption

process [45,46]. Moreover, the reduction treatment of the catalyst made the catalyst basicities decreased from 102 to 52 µmol/g for 5.0 wt.% Ni/Fe_2O_3 and 5.1 wt.% Ni/Fe_3O_4, respectively, which may be due to the possible formation of some protons during the reduction. Though not shown here, similar TPD-NH_3 characterization was also carried out over the Ni/Fe_3O_4 catalysts. Almost no NH_3 desorption peak on the TPD-NH_3 curves could be observed. These TPD-CO_2 (or NH_3) results showed that these catalysts have weak or almost no acidities, but possessed weak and medium basicities. Particularly when nickel species was incorporated into the iron oxide, the basicity of iron oxide would be remarkably enhanced.

3.2. Catalytic activity testing

First, the reaction of HDA and EC in ethanol as the model reaction for corresponding N-substituted carbamates was conducted over NiO_x, Fe_3O_4, and Ni/Fe_3O_4 with varied Ni content, Table 3. In the blank test or in presence of pure NiO_x or Fe_3O_4 (entries 1–3), the selectivities for diethyl hexamethylenedicarbamate (EHDC) were 20–72%, although the HDA conversions were all nearly 100%. It means that the role of the catalyst is to enhance the selectivity of EHDC and not the conversion of amine. The main by-product was white solid and was defined as polyurea with FT-IR analysis with a peak at 1616 cm^{-1}, which could be attributed to carbonyl group of polyurea compounds [47]. Except polyurea by-product, $C_2H_5OC(O)OC_2H_5$ and $C_2H_5NHC(O)OC_2H_5$ were also detected with GC–MS. The selectivities for EHDC were greatly improved when nickel component was introduced into the iron oxide and increased with the increasing nickel content, entries 4–6. For example, 98% of selectivity and isolated yield could be achieved over 5.1 wt.% Ni/Fe_3O_4. For the 5.0 wt.% Ni/Fe_2O_3, the selectivity for EHDC was 82% and lower than that of 5.1 wt.% Ni/Fe_3O_4, entry 7. Therefore, the reduction treatments of the catalyst at 400 °C under H_2 not only improve the selectivity for the EHDC but also provide a simple method for the catalyst separation using external magnetic field. These results suggested that the reduction treatment of the catalyst would greatly enhance the catalyst performance. Moreover, the selectivity for EHDC was only 62% when the mechanical mixture of iron oxide (94.9 wt.%) and nickel oxides (5.1 wt.%) was used as catalyst (entry 9), which was similar as that using iron oxide or nickel oxide as catalyst individually. Thus, the synergism between nickel oxide and iron oxide

Table 3
Results of EHDC syntheses over different catalysts.[a]
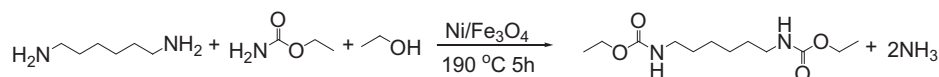
Entry	Catalyst	Conversion (%)	Selectivity (%)		Yield/%[c]	TON[d]
			EHDC	By-products [b]		
1	None	>99	20	80	20	–
2	NiO_x	>99	52	48	52	4000
3	Fe_3O_4	>99	72	28	72	2250
4	1.1 wt.% Ni/Fe_3O_4	>99	78	22	78	–
5	3.2 wt.% Ni/Fe_3O_4	>99	92	8	92	2140
6	5.1 wt.% Ni/Fe_3O_4	>99	98	2	98	1885
7	5.0 wt.% Ni/Fe_2O_3	>99	82	18	82	804
8	Used 5.1 wt.% Ni/Fe_3O_4	>99	96	4	96	1655
9	NiO_x + Fe_3O_4 (95 wt.%)	>99	62	38	62	–
10	MgO	>99	58	42	58	–

[a] Reaction conditions: HDA, 10 mmol; EC, 70 mmol; ethanol, 170 mmol; catalyst, 100 mg; reaction temperature, 190 °C; reaction time, 5 h.
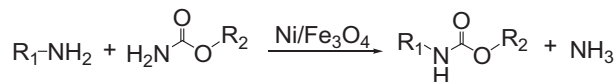[b] Polyurea derivatives.
[c] Isolated yield based on charged HDA.
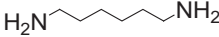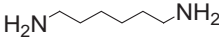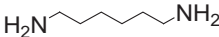[d] TON: mol of EHDC/mol of basic site.
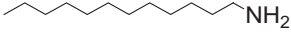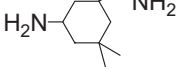
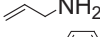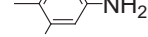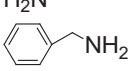during catalyst preparation is crucial to get active enough catalyst. Additionally, although the obtained results did not support the previously reported mechanism of leaching provided the catalytically relevant species in solution and the operation of the solid played as a reservoir [48], it could not be ruled out conclusively at present, and the detailed catalytic mechanism will be investigated next. Since the TPD-CO_2 results showed that increasing nickel content into the Fe_3O_4, the total basic sites would be increased, it can be conjectured that the catalyst with more basic sites was helpful to increase the EHDC selectivity. Based on this hypothesis, we adopt the solid base MgO as catalyst (entry 10), which has more basic sites than that of Ni/Fe_3O_4. However, the selectivity of EHDC was only 58%, which suggested that the specific kind and amount of basic sites, but not the all of basic compounds, might be the major reason for the high catalytic activity of Ni/Fe_3O_4. Moreover, the reaction and TPD-CO_2 results of 5.0 wt.% Ni/Fe_2O_3 also suggested that the catalyst performance was not closely proportional to catalyst basicity. Since the Ni/Fe_3O_4 is magnetic, it is worth noting that such catalyst could be easily separated and recovered using an external magnetic field and could be recycled for at least five times with stable activity, entry 8. Additionally, the TOF of our catalyst was only 0.1S^{-1}, suggesting that the reaction rate was relatively lower, and this was consistent with the small BET surface area of the catalyst. Although surface area is relatively lower, the 5.1 wt.% Ni/Fe_3O_4 catalyst intrinsically possessed higher catalytic activity for the N-substituted carbamates synthesis. It can be expected that the reaction rate could be accelerated if the catalyst surface area is further increased.

3.3. Generality of the catalysts

In order to investigate the limitation and scope of the catalysts, reactions between various amines such as HDA, 4,4′-methylenedicyclohexanamine, isophorondiamine, dodecylamine, allylamine, MDA, 2,4-diaminotoluene, and benzylamine with MC (or EC and BC) for corresponding N-substituted carbamates were further tested over 5.1 wt.% Ni/Fe_3O_4, Table 4. First, the impact of variation of alkyl carbamates as carbonyl source on the HDA reaction for corresponding N-substituted carbamates was tested, entries 1–3. 96%, 98% and 90% of isolated yields of the corresponding N-substituted carbamates were obtained, indicating that EC as carbonyl source was better than those of MC and BC. When the dodecylamine used as other substrate, entries 4–6, the following reactivity order was obtained: EC ⩾ MC > BC, which was consistent with the HDA used as substrate. Our experimental results suggested that the yields of the corresponding N-substituted carbamates have less related with the reactivities of MC, EC, or BC but much related with the reactivities of O-methyl from methanol, O-ethyl from ethanol, and O-butyl from butanol during further alcoholysis of the urea intermediate. The nucleophilicity and steric hindrance of the O-methyl, O-ethyl, and O-butyl are in the following order: O-butyl > O-ethyl > O-methyl. Considering a balance of those two effects, O-ethyl would have relatively higher reactivity during further alcoholysis of the urea intermediate. Then, various aliphatic amines and EC as substrates were further investigated, entries 6–9. Although the conversions of various aliphatic amines were all nearly 100%, the isolated yields of the corresponding N-substituted carbamates of

Table 4
Scope and limitation of 5.1 wt.% Ni/Fe_3O_4 for catalytic syntheses various N-substituted carbamates.[a]

$$R_1-NH_2 + H_2N \overset{O}{\underset{O}{\parallel}} R_2 \xrightarrow{Ni/Fe_3O_4} R_1 \overset{O}{\underset{H}{N}} \overset{O}{\underset{O}{\parallel}} R_2 + NH_3$$

Entry	Substrates	Carbonyl sources	Conversion (%)	Selectivity (%)		Yield[c] (%)	TON[d]
				Product	By-products[b]		
1	H₂N~~~~NH₂	EC	>99	98	2	98	1885
2	H₂N~~~~NH₂	MC	>99	96	4	96	1846
3	H₂N~~~~NH₂	BC	>99	90	10	90	1731
4	~~~~~NH₂	MC	>99	96	4	96	1846
5	~~~~~NH₂	BC	>99	91	9	91	1750
6	~~~~~NH₂	EC	>99	98	2	98	1885
7	H₂N-⬡-⬡-NH₂	EC	>99	92	8	92	1769
8	H₂N-⬡(NH₂)	EC	>99	94	6	94	1808
9	⸝⸝NH₂	EC	>99	99	1	98	1885
10	H₂N-⬡-CH₂-⬡-NH₂	EC	97	95	5	92	1769
11	⬡(NH₂)(H₂N)	EC	96	94	6	90	1731
12	⬡-CH₂NH₂	EC	99	94	6	93	1788

[a] Reaction conditions: entries 1–9, amine 10 mmol; alkyl carbamate 70 mmol; alcohol 170 mmol; catalyst, 100 mg; reaction temperature, 190 °C; reaction time, 5 h; entries 10–12, reaction time 12 h.
[b] By-products mainly include polyurea derivatives, as well as a few N-ethylated aromatic amine.
[c] Isolated yield based on charged amine.
[d] TON: mol of N-substituted carbamate/mol of basic site.

diamines (92–94%) were slightly lower than those of monoamine (98%), which could be ascribed to the high steric hindrance of diamines caused by the cyclic structure. Finally, the reaction of various aromatic amines and EC was also studied, entries 10–12. The results showed that the conversion (96–99%) of aromatic amines and the isolated yields (90–93%) of the corresponding N-substituted carbamates were lower than that of aliphatic amines, even though the reaction times prolonged to 12 h. Furthermore, the N-ethylated aromatic amine was detected when the aromatic amines used as substrate. The formed N-ethylated aromatic amine should be related to the reaction between aromatic amine and diethyl carbonate formed via EC alcoholysis. All those results suggested that the reaction of alkyl carbamates with aliphatic amines was easier than with aromatic amines, which should be attributed to the nucleophilicity difference in the two types of amines. In one word, the simple Ni/Fe₃O₄ could be a good catalyst for the syntheses of various N-substituted carbamates.

3.4. Identification of reaction pathway with quasi in situ FT-IR

There may be two possible reaction pathways for the formation of N-substituted carbamates from alkyl carbamates and amines. One is direct deamination of alkyl carbamate with amine (Scheme 2, step A) and another is through the formation of substitute urea intermediate and the N-substituted carbamate was obtained via further alcoholysis of the substituted urea (Scheme 2, step B) [30,32].

In order to explore the mechanism of the reaction, it was traced by quasi in situ FT-IR under varied temperatures. Prior to the IR test, we investigated the reaction of MDA, EC, and alcohol using
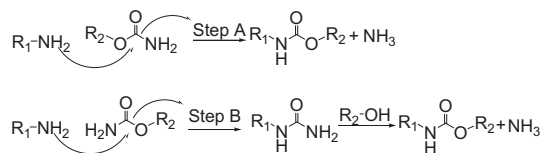
Scheme 2. Possible reaction pathway for the synthesis of N-substituted carbamate from alkyl carbamate and amine.

KBr as catalyst, and the results showed that the KBr has no effect on this reaction (not shown here). So, the IR experiments were conducted with pressed KBr. Fig. 6a showed the IR spectra evolution of the reaction mixture of MDA, EC, and catalyst with increasing the temperature. At 30 °C, the band at 1688 cm⁻¹ is assigned to the carbonyl stretch of EC and blue shift occurred with the increasing temperature [49]. When the temperature reached to 110 °C, the carbonyl band of EC split into three peaks at 1717, 1766, and 1777 cm⁻¹. The peak at 1610 cm⁻¹ also split into two peaks at 1580 and 1620 cm⁻¹. The former band is assigned to the N–H bending, which shifted from 1610 to 1580 cm⁻¹ with the increasing temperature. Such phenomena could also be observed in the IR spectra without the addition of MDA (not shown here). The later band is assigned to the carbonyl stretch of urea formed from MDA and EC [50]. These observations suggested that there existed strong interaction between the substrates and catalyst. Additionally, a new band appeared at 2170 cm⁻¹ was attributed to the formation of isocyanic acid (O=C=N stretching) through the decomposition of the EC when the temperature is higher than 150 °C [51]. Fig. 6b shows the IR spectra evolution of reaction mixture of MDA, EC, catalyst, and alcohol. In comparison with Fig. 6a, two
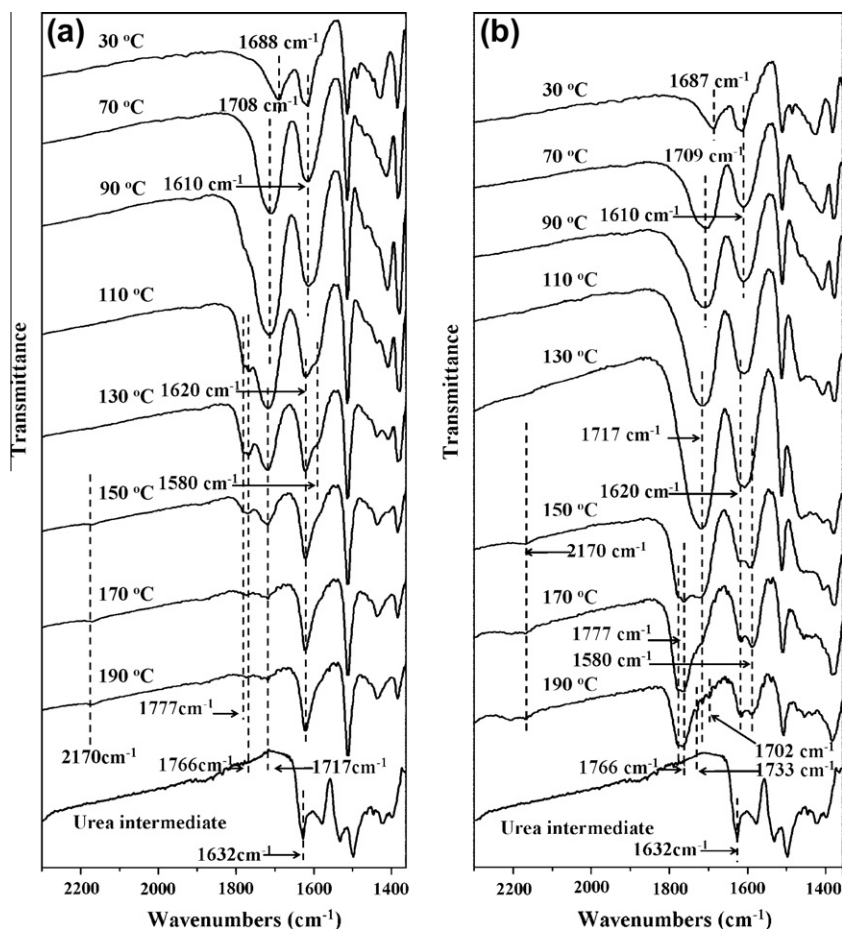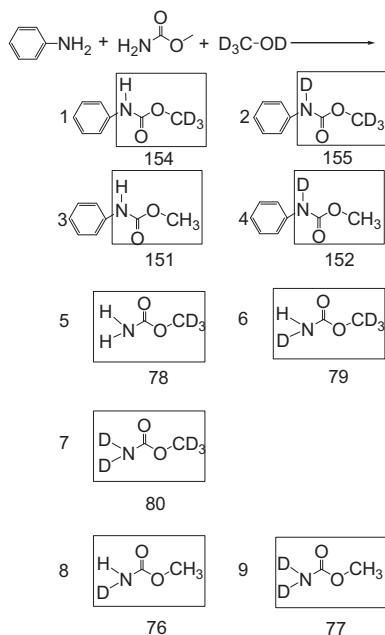
Fig. 6. FT-IR spectra evolution of: (a) EC + MDA + 5.1 wt.% Ni/Fe₃O₄ and (b) EC + MDA + 5.1 wt.% Ni/Fe₃O₄ + butanol.

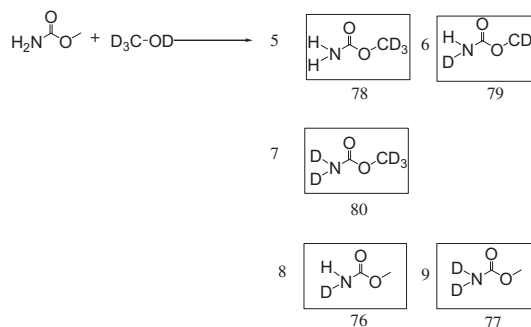**Scheme 3.** Reaction of aniline, MC, and d_4-methanol.

new peaks at 1702 and 1733 cm^{-1} appeared at 190 °C, which were consistent with the spectra of pure dibutyl-4,4′-methylenedicarbamate. Meanwhile, the intensity of the peak at 1620 cm^{-1} was much lower in comparison with the corresponding peak in Fig. 6a. These observations indicated that the N-substituted carbamate could not be formed without alcohol and the formation of substituted urea may be the key intermediate and the N-substituted carbamate was obtained via further alcoholysis of the substituted urea. Furthermore, such urea intermediate was separated and analyzed by NMR and FT-IR. The NMR results showed that the urea intermediate was what we needed. However, in the FT-IR analysis, the carbonyl stretch of urea intermediate was found at 1632 cm^{-1} (the last line in Fig. 6a and b), which was 12 cm^{-1} higher than that of quasi in situ FT-IR experiment, and this may be ascribed to the hydrogen bonding interaction between urea intermediate and butanol or MDA in the reaction mixture.

3.5. Identification of reaction pathway with isotopic tracer

Isotopic tracing is also an ideal method for mechanism investigation. Therefore, the reaction of aniline and MC with d_4-methanol was also studied (Scheme 3). This reaction provided evidence of the source of the methoxy in the final product. According to the GC–MS analysis, the major products were PhNHCO$_2$CD$_3$ **1** and PhNDCO$_2$CD$_3$ **2** (>97%, **1:2**∼1:1) and only a little amount of products **3** and **4** were produced. There are two possible ways for the formation of the compounds **1** and **2**. One is alcoholysis of the urea intermediate with d_4-methanol. Another one is the transesterification of the compounds **3** and **4** with d_4-methanol. Meanwhile, compounds **5**, **6** and **7** were also produced, which formed either by alcoholysis of the urea intermediate with d_4-methanol or by the transesterification reaction of MC and d_4-methanol. Based on the corresponding peak area, the mol ratio of MC contained —OCD$_3$ to MC contained —OCH$_3$ was as follows:

Peak area$_{(78+79+80):(75+76+77)} = 12 : 88$

Then, the reaction of MC and d_4-methanol was conducted to clarify the formation pathway of the compounds **5**, **6**, and **7** (Scheme 4). Clearly, the compounds **5**, **6**, and **7** were also formed in such a reaction and the mol ratio of MC contained —OCD$_3$ to


Scheme 4. Reaction of MC and d_4-methanol.

MC contained —OCH$_3$ was the same as the above-mentioned result. Based on these results, we can conclude that the compounds **5**, **6**, and **7** were formed through the transesterification reaction of MC and d_4-methanol. More importantly, there was only 12% transesterification products (MC contained —OCD$_3$) formed. Therefore, the compounds **1** and **2** (>97%) were formed mainly through the alcoholysis of the urea intermediate with d_4-methanol (Scheme 2, step B) and not the transesterification of the compounds **3** and **4** with d_4-methanol.

Isotope competitive reaction was carried out with aniline, MC, H$_4$-methanol, and d_4-methanol. As it was shown in Scheme 5, **1** and **2** were derived from d_4-methanol and **3** and **4** were products from H$_4$-methanol. By ion selective mass spectra calibration, their characteristic m/z^+ numbers are 154, 155, 151, and 152. Based on the corresponding peak area, the mol ratio of the compounds **3**, **4** and **1**, **2** was as follows: peak area$_{(151+152):(154+155)}$ = 48:52. Thus, a kinetic isotope effect was observed for the urea intermediate alcoholysis. The numbers of KIE were calibrated as follows (number in the bracket is the standard deviation of the results repeated three times).

$$\text{KIE} = k[\text{H}]/k[\text{D}]$$
$$= \text{product}(3) + \text{product}(4)/\text{product}(1) + \text{product}(2)$$
$$= 0.923(0.04) : 1$$

All these results indicated that the formation of substituted urea and further alcoholysis pathway were more favorable than the direct deamination pathway. The formation of N-substituted carbamate **II** takes place, thus, in two consecutive steps. The first is the formation of the urea intermediate **I** with the removal of a
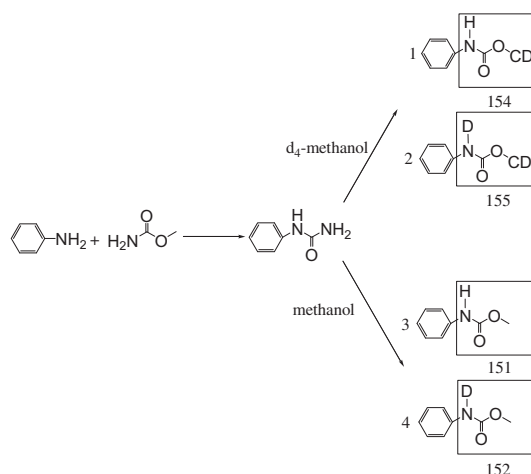
Scheme 5. An illustration of the kinetic studies by isotope competitive reactions.
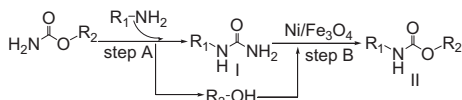
Scheme 6. Reaction pathway for synthesis of N-substituted carbamate from alkyl carbamate and amine.

molecule of alcohol (Scheme 6, step A), followed by the formation of N-substituted carbamate in the second step with the contemporary elimination of a molecule of ammonia (Scheme 6, step B).

Although the aliphatic amines as substrate for the identification of reaction pathway were not used due to its highly reactive with CO_2 and water in the air, which could be lead to some error for the results, we believe that the aliphatic amines undergo the same reaction pathway as the aromatic amines. Additional, the urea intermediate was further prepared with the reaction of HDA, EC, and ethanol without catalyst. The results showed that HDA conversion was nearly 100%, urea intermediate selectivity was 80%, and EHDC selectivity was only 20%. Then, the reactivity of urea intermediate is further studied under the same conditions with 5.1 wt.% Ni/Fe$_3$O$_4$. The results showed the conversion of urea intermediate was 90% and the EHDC yield was 90%. These suggested that the urea intermediate was formed easily and the catalyst mainly promoted the further alcoholysis of the urea intermediate.

4. Conclusions

In conclusion, a nickel-promoted magnetic iron oxide catalyst was developed for the effective syntheses of N-substituted carbamates. The catalyst could be easily isolated using external magnetic field and recovered for several runs without deactivation. In general, good to excellent yields were obtained with various amines and alkyl carbamates. Catalyst characterization results suggested the catalytic activity may be derived from the delicate synergy between Ni and Fe species resulted in specific basic sites. Reaction pathway investigations revealed that the N-substituted carbamates were formed via substitute urea intermediate and the catalyst mainly promoted the further alcoholysis of the urea intermediate.

Acknowledgment

References

[1] C.S. Schollenberger, US 2871218, 1959.
[2] P.A. Tierney, R.M. Hedrick, J.D. Gabbert, US 3833534, 1974.
[3] D.J. Goldwasser, R.W. Oertel, US 4567236, 1986.
[4] W. Henstchel, Chem. Ber. 17 (1884) 1284.
[5] Y. Liu, H. Zhao, G. Li, Isocyanate, Chemical Industry Press, Beijing, 2004. p. 16.
[6] P. Uriz, M. Serra, P. Salagre, S. Castillon, C. Claver, E. Fernandez, Tetrahedron Lett. 43 (2002) 1673.
[7] A.M. Tares, J. Weygand, Chem. Rev. 96 (1996) 2035.
[8] S. Ozaki, Chem. Rev. 72 (1972) 457.
[9] M.E. Duggan, J.S. Imagire, Synthesis 2 (1989) 131.
[10] R.A. Ligabue, A.L. Monteiro, R.F. de Souza, M.O. de Souza, J. Mol. Catal. A: Chem. 157 (2000) 73.
[11] B. Corain, J. Organomet. Chem. 19 (1978) 57.
[12] Y.Y. Wigfield, Int. J. Food Sci. Technol. 77 (1996) 1501.
[13] A.J. Wills, Y.K. Ghosh, S. Balasubramanian, J. Org. Chem. 67 (2002) 6646.
[14] J.P. Mayer, G.S. Lewis, M.J. Cuetius, J. Zhang, Tetrahedron Lett. 38 (1997) 8455.
[15] F. Shi, Y. Deng, J. Catal. 211 (2002) 548.
[16] P. Wehman, P.C.J. Kamer, P.W.N.M. van Leeuwen, Chem. Commun. 2 (1996) 217.
[17] F. Ragaini, S. Cenini, J. Mol. Catal. A: Chem. 161 (2000) 31.
[18] R. Juárez, P. Concepción, A. Corma, V. Fornés, H. García, Angew. Chem., Int. Ed. 49 (2010) 1286.
[19] T. Baba, M. Fujiwara, A. Oosaku, A. Kobayashi, R.G. Deleon, Y. Ono, Appl. Catal. A 227 (2002) 1.
[20] M. Aresta, A. Dibenedetto, E. Quaranta, M. Boscolo, R. Larsson, J. Mol. Catal. A: Chem. 174 (2001) 7.
[21] M. Yoshida, N. Hara, S. Okuyama, Chem. Commun. 2 (2000) 151.
[22] A. Ion, C. Van Doorslaer, V. Parvulescu, P. Jacobs, D. De Vos, Green Chem. 10 (2008) 111.
[23] C. Yokoyama, Y. Kawase, N.S. Kitakawa, R.L. Smith, J. Appl. Polym. Sci. 89 (2003) 3167.
[24] A. Behr, Angew. Chem., Int. Ed. 27 (1988) 661.
[25] M. Shi, K.M. Nicholas, J. Am. Chem. Soc. 119 (1997) 5057.
[26] F. Shi, Y. Deng, T. SiMa, J. Peng, Y. Gu, B. Qiao, Angew. Chem., Int. Ed. 42 (2003) 3257.
[27] R. Nomura, Y. Hasegawa, M. Ishimoto, T. Toyosaki, H. Matsuda, J. Org. Chem. 57 (1992) 7339.
[28] P. Heitkamper, K. Konig, R. Findeisen, US 4388238, 1983.
[29] M. Wang, H. Wang, N. Zhao, W. Wei, Y. Sun, Catal. Commun. 7 (2006) 6.
[30] Q. Li, J. Wang, W. Dong, M. Kang, X. Wang, S. Peng, J. Mol. Catal. A: Chem. 212 (2004) 99.
[31] H. Zhang, X. Guo, Q. Zhang, Y. Ma, H. Zhou, J. Li, L. Wang, Y. Deng, J. Mol. Catal. A: Chem. 296 (2008) 36.
[32] X. Guo, J. Shang, X. Ma, J. Li, H. Zhang, X. Cui, F. Shi, Y. Deng, Catal. Commun. 10 (2009) 1248.
[33] Y. Pei, H. Li, H. Liu, Y. Zhang, Catal. Today 148 (2009) 373.
[34] S. Luo, X. Zheng, J. Cheng, Chem. Commun. 44 (2008) 5719.
[35] A. Lu, W. Schmidt, N. Matoussevitch, H. Bonnemann, B. Spliethoff, B. Tesche, E. Bill, W. Kiefer, F. Schuth, Angew. Chem., Int. Ed. 43 (2004) 4303.
[36] J.F. Moulder, W.F. Stickle, P.E. Sobol, K.D. Bomben, Handbook of X Ray Photoelectron Spectroscopy, Perkin-Elmer Corporation, Eden Prairie, MN, 1992. p. 81.
[37] K. Wandelt, Surf. Sci. Reports 2 (1982) 1.
[38] M.M. Natile, A. Glisenti, Chem. Mater. 15 (2003) 2502.
[39] M.M. Natile, A. Glisenti, Chem. Mater. 14 (2002) 4895.
[40] J. Kugai, S. Velu, C. Song, Catal. Lett. 101 (2005) 255.
[41] A. Venugopal, M.S. Scurrell, Appl. Catal. A 258 (2004) 241.
[42] S.K. Banerjee, W. O'Reilly, C.E. Johnson, J. Appl. Phys. 38 (1967) 1289.
[43] J.W. Niemantsverdriet, Spectroscopy in Catalysis: An Introduction, Wiley-VCH, 2007.
[44] E. Jartych, J. Magn. Magn. Mater. 265 (2003) 176.
[45] T. Yamaguchi, Y. Wang, M. Komatsu, M. Ookawa, Catal. Surv. Jpn. 5 (2002) 81.
[46] V. Cortés Corberán, L.G. Tejuca, A.T. Bell, J. Mater. Sci. 24 (1989) 4437.
[47] R.G. Deleon, A. Kobayashi, T. Yamauchi, J. Ooishi, T. Baba, M. Sasaki, F. Hiarata, Appl. Catal. A 225 (2002) 43.
[48] U. Arnold, W. Habicht, M. Döring, Adv. Synth. Catal. 348 (2006) 142.
[49] G.G. Suchkova, L.I. Maklakov, Vib. Spectrosc. 51 (2009) 333.
[50] C.G. Cannon, J. Phys. Chem. 80 (1976) 1247.
[51] P. Hauck, A. Jentys, J.A. Lercher, Appl. Catal. B 70 (2007) 91.